

## Observations of the Relationship between 700-mb Temperatures and Severe Weather Reports across the Contiguous United States

MATTHEW J. BUNKERS, JOHN R. WETENKAMP JR., AND JEFFREY J. SCHILD

*NOAA/National Weather Service, Rapid City, South Dakota*

ANTHONY FISCHER

*NOAA/Aviation Weather Center, Kansas City, Missouri*

(Manuscript received 15 July 2009, in final form 21 October 2009)

### ABSTRACT

The relationship between 700-mb temperatures and convective severe storm reports is examined using data from 1993 to 2006 for the contiguous United States. Severe storm reports are used as a rough “proxy” for the occurrence of deep moist convection, and spatial and temporal distributions of 700-mb temperatures associated with these reports are analyzed. Secondly, the distributions are assessed by individual severe storm report type, and convective inhibition also is evaluated. The motivation for this study is derived from the occasionally used 10°–12°C at 700 mb rule of thumb for estimating the extent and strength of the capping inversion. Whereas there is a semblance of merit for using this rule at times, its utility is shown to be strongly dependent on 1) geographic location, particularly with respect to surface elevation and the frequency of elevated mixed layers, and 2) the time of year. Calculation of convective inhibition, careful examination of the sounding, and assessment of lifting mechanisms likely are more valuable than 700-mb temperatures when forecasting the potential for deep moist convection and severe storms.

### 1. Introduction

Forecasting whether a capping inversion will give way to deep moist convection (DMC) remains a difficult problem for operational forecasters (Moller 2001, 437–438; Wakimoto and Murphey 2009, 912–913). Actually, this is a two-pronged problem (McNulty 1995): Will thunderstorms initiate in a given area, or will mature thunderstorms be able to move into a given area? This study will discuss some of the variables used to evaluate the capping inversion, starting with modern approaches, and then focusing on 700-mb temperatures ( $T_{700}$ ).

Convective inhibition (CIN; Colby 1984) is a diagnostic variable that is used to assess the strength of the capping inversion. CIN is a measure of the energy associated with negatively buoyant air that rising parcels need to overcome in order to reach the level of free convection (LFC)—ultimately resulting in DMC once the LFC is reached. This negative energy typically is overcome

through mesoscale and storm-scale processes, such as those brought about by boundaries, differential heating, and terrain influences (e.g., McNulty 1995; Moller 2001; Weckwerth and Parsons 2006; Kalthoff et al. 2009). These boundaries, usually marked by some horizontal temperature contrast at lower to middle levels, can allow for transverse vertical circulations such that DMC is initiated as air travels out from underneath a capping inversion, near the edge of the lid (Carlson 1998, 470–473).

Given the relative paucity of upper-air observations in time and space, today’s forecasters often utilize numerical models when trying to anticipate CIN. Even though the model resolution is desirable, Moller (2001) stated that model forecasts can produce CIN fields with considerable noise and uncertainty, which is in large part due to difficulties in properly measuring and forecasting low-level moisture (Weckwerth and Parsons 2006). Indeed, even model initial *analyses* of CIN can be plagued with inconsistencies (e.g., cf. the four different model analyses in Fig. 1). To complicate matters further, some software programs report notably different CIN values for the same sounding. For example, when two LFCs are present (e.g., Fig. 2), one program might report the lower

---

*Corresponding author address:* Dr. Matthew J. Bunkers, National Weather Service, 300 East Signal Dr., Rapid City, SD 57701-3800.  
E-mail: matthew.bunkers@noaa.gov

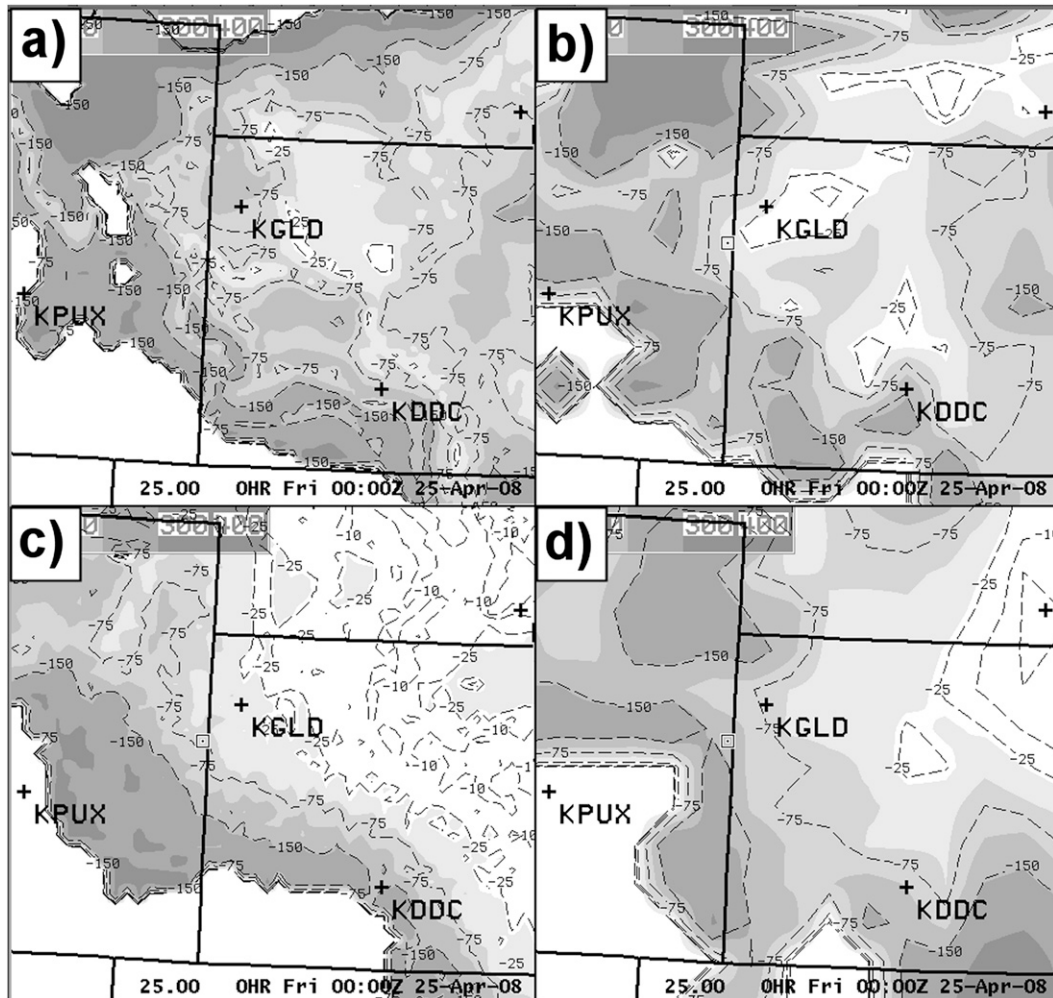


FIG. 1. Model initial analyses of the surface-based CIN ( $\text{J kg}^{-1}$ ) valid 0000 UTC 25 Apr 2008 for the area centered on western KS. Models include the (a) Local Analysis and Prediction System (LAPS), (b) Rapid Update Cycle (RUC), (c) North American Mesoscale (NAM), and (d) Global Forecasting System (GFS). Values of SBCIN  $< -30 \text{ J kg}^{-1}$  are shaded, with the darkest shading representing SBCIN  $< -250 \text{ J kg}^{-1}$ .

CIN-LFC pair while the other program reports the upper CIN-LFC pair. Similarly, some programs apply the virtual temperature correction (Doswell and Rasmussen 1994; information also online at <http://www.flame.org/~cdoswell/virtual/virtual.html>), which can result in non-trivial differences in CIN (e.g., Fig. 3).

Shortly after Colby (1984) introduced CIN, Graziano and Carlson (1987) evaluated the lid strength index [LSI, introduced by Carlson et al. (1980)] as a tool to quantify the capping inversion. They defined the LSI as the difference between the maximum saturation wet-bulb potential temperature at the warmest point in the inversion ( $\theta_{sw1}$ ) and the vertically averaged value of the wet-bulb potential temperature in the layer between 30 and 80 mb above ground ( $\bar{\theta}_w$ ). The 90th percentile of the LSI from their study of DMC was  $2.0^\circ\text{C}$ , indicating a minimal

probability of DMC when the LSI exceeds  $2.0^\circ\text{C}$ . Graziano and Carlson (1987) also found a paradoxical relationship whereby DMC is more likely when the LSI is small (near zero), yet the probability of severe local storms—conditional on DMC—increases with increasing LSI for a given value of buoyancy. The usage of CIN has prevailed over the LSI in the operational and research communities since the inception of these indices, perhaps because CIN is an integrated quantity instead of being dependent on a subset of sounding levels like the LSI.

Before the advent of more sophisticated computers and software routines in the 1990s—which enabled the routine calculation of CIN—forecasters considered  $T_{700}$  to be a simple guide for predicting the strength of the capping inversion. One reason for this is that, away from mountainous areas, the 700-mb level often is slightly

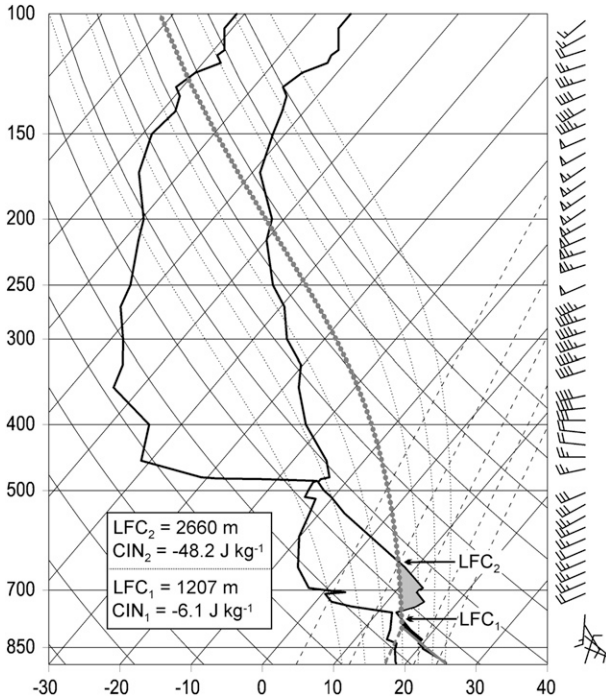


FIG. 2. Observed skew  $T$ - $\log p$  sounding (thick black lines) for Rapid City, SD, valid 1800 UTC 25 Jul 2001. Half, whole, and flag wind barbs denote 2.5, 5, and 25  $\text{m s}^{-1}$ , respectively. Temperature is given along the abscissa ( $^{\circ}\text{C}$ ) and pressure is plotted along the ordinate (mb). The ascent for the 1000-m mixed-layer parcel is highlighted by the thick gray lines. The small black shaded region represents  $\text{CIN}_1$  and the larger gray-shaded region represents  $\text{CIN}_2$  based on this mixed-layer parcel.

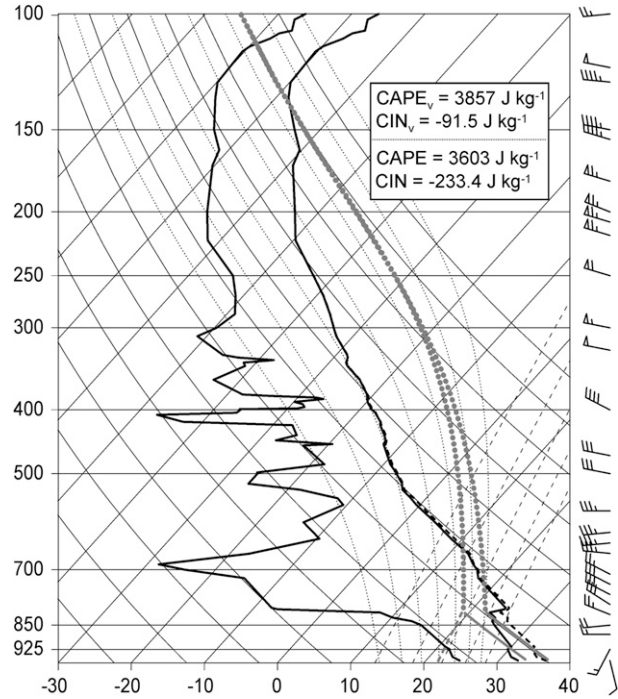


FIG. 3. Observed skew  $T$ - $\log p$  sounding (thick black lines) for Aberdeen, SD, valid 0000 UTC 14 Aug 2007, similar to Fig. 2. The virtual temperature is given as the thick dashed black line. The ascent curves for both the (left) uncorrected and (right) corrected 1000-m mixed-layer parcels are indicated by the thick gray lines. The subscripts indicate that the virtual temperature correction was applied (i.e.,  $\text{CAPE}_v$  and  $\text{CIN}_v$ ).

above the mean height of the typical capping inversion. Since 700 mb also is a mandatory pressure level for radiosonde observations, this offers a convenient means of roughly estimating the capping inversion. In favor of this, an analysis of long-term records from seven sounding sites across mainly the central contiguous United States (CONUS, starred locations in Fig. 4) indicates that  $T_{700}$  is significantly correlated with CIN and the LSI (Table 1), but generally with weaker correlations for stations at the lowest elevations (as discussed further in section 3). Since CIN is defined as negative herein, a negative correlation between  $T_{700}$  and CIN indicates higher temperatures are associated with stronger capping.

Evidence for using  $T_{700}$  as a proxy for the capping inversion goes back to at least the 1950s. Means (1952, p. 173) suggested that “Thunderstorm activity seems to be damped under the warm ‘lid’ aloft at 700 mb. . . .” Miller (1967, p. 6-4) later quantified this by stating: “During summer months the more significant storms appear to form north and northeast of the +10 to +14 [ $^{\circ}\text{C}$ ] isotherms at the 700-mb level.” Johns and Doswell

(1992, p. 593) pointed out several limiting factors to DMC, one of which includes the following: “Deep convection is usually limited to those areas where the forecast 700-mb temperature (NGM) is colder than  $12^{\circ}\text{C}$ .” Johns and Doswell further cautioned that this empirical rule—which relates to the strength of the capping inversion, or CIN—does not apply at high surface elevations where the 700-mb level becomes part of the mixed layer. In accord with the above references, Junker et al. (1999) indicated that “Forecasters at HPC and the Storm Prediction Center have long used 700-mb temperatures of  $12^{\circ}\text{C}$  or warmer as an indicator that a strong cap generally would inhibit the development of a convective system.” Other instances of this  $T_{700}$  rule of thumb can be found in Schaefer (1986,  $12^{\circ}\text{C}$ ) and Byrd (1993,  $10^{\circ}\text{C}$ , eastern part of the Great Plains); R. Maddox (2009, personal communication) indicated that  $10^{\circ}\text{C}$  was used at the Military Weather Warning Center during the late 1960s and early 1970s for locations east of  $100^{\circ}\text{W}$ —unless the atmosphere was of a tropical character or unless very strong forcing was expected. These references likewise suggest the rule of thumb was not intended to be applied to the mountainous western CONUS.

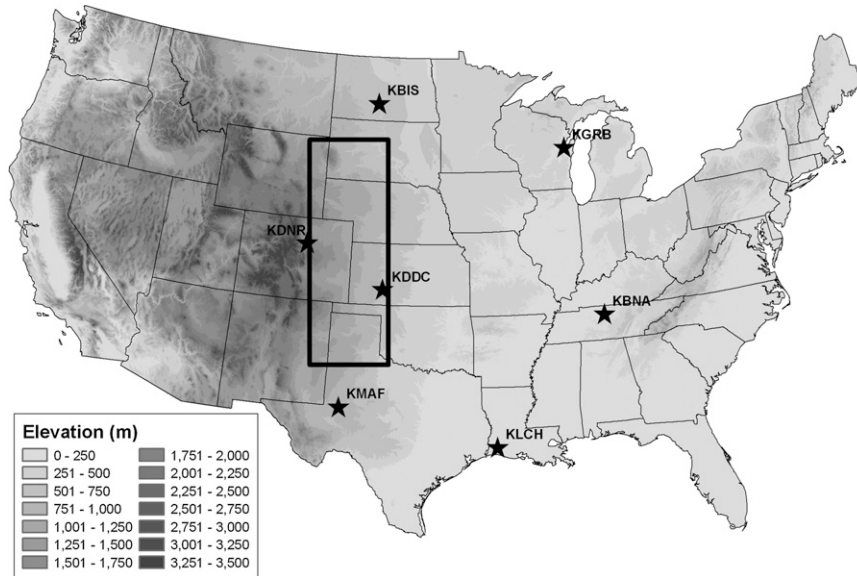


FIG. 4. Elevation map (m) of the CONUS, which encompasses the study area herein. Stars represent radiosonde locations used for the correlation analysis in Table 1, and the box denotes the “high plains” region, which was used for the cumulative frequency analysis in Fig. 7.

In addition to these references, there is a plethora of informal Internet-based materials pertaining to this subject.<sup>1</sup> An Internet search, as well as our anecdotal operational evidence gained from reading many forecast discussions, suggests that—although CIN remains more widely utilized—the use of  $T_{700}$  to identify the capping inversion has not diminished in recent years, perhaps because of complications surrounding model forecasts of CIN as noted above. In particular, the 10°–12°C isotherms at 700 mb have been used as a loose discriminator between environments with “storms” and those with “no storms,” especially during the warmest months of May, June, July, and August. Seasonally varying temperature thresholds also are cited in some informal references (e.g., Davies 2009). In spite of this usage, one can find soundings associated with DMC that display high  $T_{700}$ , but with minimal CIN (e.g., Fig. 5a;  $T_{700} > 17^{\circ}\text{C}$ ). Conversely,  $T_{700}$  may be well below the perceived “threshold” value, yet the CIN is exceptional and thus DMC is precluded (e.g., Fig. 5b;  $T_{700} < 6^{\circ}\text{C}$ ). These two examples provide motivation for eschewing 10°–12°C at 700 mb as a primary capping discriminator.

The purpose of this note is twofold: 1) to provide a climatology so forecasters have a reference in case they

choose to use  $T_{700}$  as an ancillary guide to CIN for capping and forecasting DMC and severe storms; and 2) to remind forecasters that many severe storms do occur when  $T_{700}$  is well above 10°–12°C, emphasizing the use of  $T_{700}$  within the framework of broader conceptual models and seasonal guidelines rather than as a singular concrete rule. This will be done in a circuitous fashion by examining severe storm reports, which are predicated on convective initiation; the caveats of this methodology are discussed in section 2. While other parameters such as CIN or the LSI may generally prove more effective for evaluating the strength of the capping inversion,<sup>2</sup>  $T_{700}$  can still provide useful information when gauging the relative warmth of the capping inversion above the boundary layer. For example, it may be that  $T_{700}$  provides a potential upper bound on DMC and severe storms. It is further hypothesized that  $T_{700}$  could have utility in anticipating the severe weather threat type, such that  $T_{700}$  might be higher for severe wind than for severe hail (e.g., Byrd 1993). For these reasons, in addition to the perceived misuse of  $T_{700}$ , we believe it is important to

<sup>1</sup> An Internet search for “700mb temps capping” will bring up a myriad of examples with 700-mb temperatures used in discussions that are related to thunderstorm development/occurrence.

<sup>2</sup> Visible satellite images can provide useful qualitative information on the strength of capping inversions, in particular for short-term (0–3 h) forecasts. For example, interactions of horizontal convective rolls with other boundaries often portend DMC (Weckwerth and Parsons 2006), whereas laminar billow/wave clouds are a good indicator of a stable boundary layer (Bikos et al. 2002)—and thus a limited potential for DMC.

TABLE 1. Correlation coefficients between  $T_{700}$  and various capping indices for seven sounding sites, ordered by decreasing elevation from left to right [DNR; MAF; DDC; BIS; GRB; WI (GRB); Nashville, TN (BNA); and Lake Charles, LA (LCH)]. The first of the three correlation coefficients is for all soundings, the second value is for all 0000 UTC soundings, and the third value is for all 1200 UTC soundings. Coefficients  $>0.05$ – $0.06$  are significantly ( $\alpha < 0.001$ ) different from zero based on a Student's  $t$  test (Wilks 1995). Soundings from 1948 to 2008 that possessed SBCAPE  $> 50 \text{ J kg}^{-1}$  were used in the calculations, except only the 1953–2008 period was available for GRB and MAF. A parcel with averaged values of  $\theta$  and a mixing ratio in the lowest 1000 m was used for the mixed-layer (ML) calculations; MU refers to the most unstable parcel/level in the lowest 300 mb of the sounding; and SB refers to the surface-based parcel. The virtual temperature correction (Doswell and Rasmussen 1994) was used for all parcel calculations.

Correlations	DNR	MAF	DDC	BIS	GRB	BNA	LCH
(All/0000 UTC/1200 UTC)							
$T_{700}$ vs MLCIN	-0.29/-0.25/-0.65	-0.31/-0.12/-0.56	-0.36/-0.23/-0.59	-0.50/-0.44/-0.68	-0.36/-0.32/-0.40	-0.19/-0.14/-0.26	-0.14/-0.11/-0.18
$T_{700}$ vs MUCIN	-0.24/-0.21/-0.49	-0.27/-0.08/-0.48	-0.31/-0.16/-0.49	-0.41/-0.39/-0.48	-0.26/-0.24/-0.23	-0.13/-0.08/-0.18	-0.09/-0.06/-0.14
$T_{700}$ vs SBCIN	-0.25/-0.23/-0.60	-0.28/-0.08/-0.54	-0.33/-0.16/-0.64	-0.45/-0.41/-0.69	-0.34/-0.29/-0.48	-0.20/-0.09/-0.39	-0.08/-0.03/-0.15
$T_{700}$ vs LSI	0.05/0.09/0.66	0.28/0.06/0.67	0.43/0.32/0.72	0.47/0.40/0.66	0.19/0.13/0.31	0.08/-0.03/0.24	0.21/0.18/0.26

quantify this rule of thumb that apparently has been, and continues to be, at least moderately used.

### 2. Data and methods

All convective severe storm reports for March–October from 1993 to 2006 for the CONUS (Fig. 4) were obtained from the National Oceanic and Atmospheric Administration (NOAA) *Storm Data* resource using the SVRLOT software (Hart 1993; software available online at <http://www.spc.noaa.gov/software/svrplot2/>). This search yielded 297 086 reports (Table 2), most of which are confined to the eastern two-thirds of the CONUS [similar to Brooks et al. (2003, their Fig. 4) and Doswell et al. (2005, their Figs. 5 and 6)]. Some of the severe wind reports from 1993 to 2002 were listed as “damage” instead of possessing a numerical value; herein these were assigned a nominally severe value of  $25.7 \text{ m s}^{-1}$  (50 kt), which may be an overestimate in some cases where shallow-rooted trees in moist soil were toppled by subsevere winds. The severe reports then were subdivided into “significant” categories according to the criteria of Hales (1988): tornado rating  $\geq \text{F2}$ , hail with diameter  $\geq 5.1 \text{ cm}$  (2 in.), and wind gusts  $\geq 33.4 \text{ m s}^{-1}$  (65 kt). This resulted in 1400 significant tornado reports, 7137 significant hail reports, and 9411 significant wind reports (Table 2), which collectively comprise 17 948 (or 6%) of all severe reports herein.

Next, using the 3-h, 32-km gridded North American Regional Reanalysis (NARR; Mesinger et al. 2006), each individual severe report was matched nearest in time and space with (i) the value of  $T_{700}$  and (ii) the most unstable CIN (MUCIN<sup>3</sup>) in the layer between the surface and 180 mb above ground. While the primary focus of the present study is on  $T_{700}$  and severe storm reports, MUCIN also is considered since it is a more robust measure of the capping inversion than is  $T_{700}$  (i.e., it is an integrated quantity associated with the energy needed to overcome the cap; see section 1). Although surface-based CIN (SBCIN) also is available from the NARR, MUCIN was chosen because it is better suited to collectively represent both surface-based and elevated (e.g., Corfidi et al. 2008) forms of DMC. Additionally,

<sup>3</sup> To find the most unstable “parcel,” the lowest 180 mb of the NARR atmosphere is divided into six 30-mb-deep layers, and then the average thermodynamics are computed for each 30-mb layer (without applying the virtual temperature correction). The layer with the largest equivalent potential temperature ( $\theta_e$ ) is lifted using that layer’s values to compute the MUCIN (G. Manikin 2009, personal communication), which has attributes of mixed-layer CIN. This is not be confused with the MUCIN methodology given in Table 1.

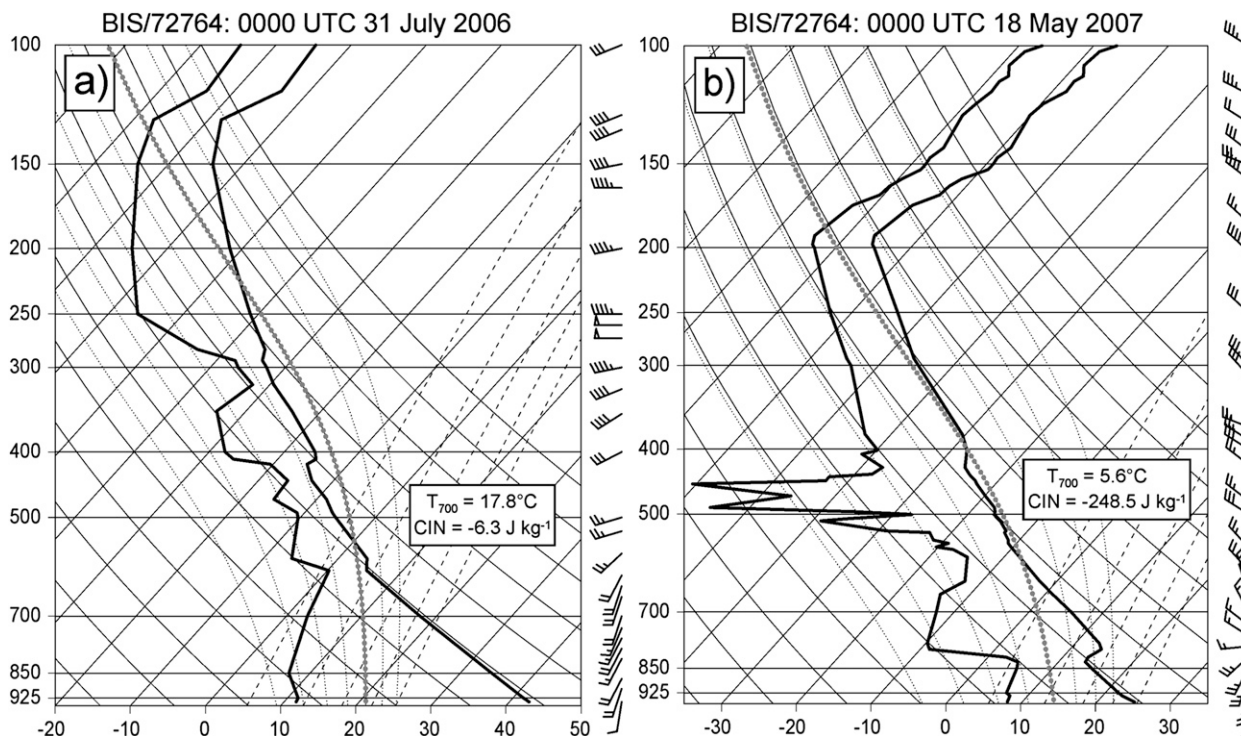


FIG. 5. Observed skew  $T$ - $\log p$  soundings (thick solid lines) for Bismarck, ND, valid (a) 0000 UTC 31 Jul 2006 and (b) 0000 UTC 18 May 2007, similar to Fig. 2. The moist adiabat for the 1000-m mixed-layer parcel is highlighted by the bold gray dotted line.

the NARR MUCIN has characteristics of mixed-layer CIN (because of averaging), which makes it less sensitive to “data spikes.”

Using geographic information system (GIS) software, the spatial distributions of the maximum and average  $T_{700}$  for a variety of report combinations (e.g., all hail, significant tornadoes, 1800–0600 UTC, etc.) were derived across the CONUS for a grid with spacing of roughly 80 km (e.g., Brooks et al. 2003; Doswell et al. 2005; Ashley et al. 2008). The same process was repeated for the MUCIN data, except that the minima were computed instead of the maxima (because CIN is defined as

negative herein). At least five reports were required per grid box, with the exception of significant tornadoes where only one report was required per grid box. This latter constraint was a trade-off between sample size (Table 2, cf. the “sig” values in the last row) and geographical coverage; the entire significant tornado grid is only 25% of the area of the entire significant hail grid if five reports per grid box are required for both. This methodology dictates that caution must be used when interpreting the results for the significant tornado dataset. Because of this, monthly distributions were not constructed for the significant categories.

TABLE 2. Convective severe storm reports from 1993 to 2006 that were used in the present study (297 086 total). Significant severe weather reports in parentheses are as defined in Hales (1988): “sig. torn.” includes F2–F5 tornadoes, “sig. hail” includes hail with diameter  $\geq 5.1$  cm (2.0 in.), and “sig. wind” includes wind gusts  $\geq 33.4$  m  $s^{-1}$  (65 kt).

	Tornado (sig. torn.)	Hail (sig. hail)	Wind (sig. wind)	Total (all sig.)
March	939 (165)	10 094 (362)	5499 (385)	16 532 (912)
April	2087 (276)	23 948 (1136)	11 384 (850)	37 419 (2262)
May	3786 (381)	36 625 (2070)	23 089 (1766)	63 500 (4217)
June	3242 (201)	30 532 (1587)	32 870 (2344)	66 644 (4132)
July	1986 (118)	19 408 (1031)	34 675 (2228)	56 069 (3377)
August	1223 (72)	12 992 (533)	20 760 (1278)	34 975 (1883)
September	1140 (102)	6086 (255)	6557 (360)	13 783 (717)
October	887 (85)	3567 (163)	3710 (200)	8164 (448)
Total	15 290 (1400)	143 252 (7137)	138 544 (9411)	297 086 (17 948)

Additional nine-point smoothing of the  $T_{700}$  and MUCIN data was applied in order to bring out more clearly the spatial pattern in the results. This process mitigated the effects of relatively data-sparse areas by allowing them to be influenced by neighboring grids containing more robust data. On the other hand, local extrema sometimes were reduced modestly when surrounded by valid boxes with relatively few reports—such that the extrema in neighboring boxes likely were not captured. The net effect is that when viewing the monthly smoothed data, local maxima of  $T_{700}$  tend to be reduced by  $0.75^{\circ}$ – $1.75^{\circ}\text{C}$  over the raw data; this is equivalent to the standard deviation of the differences between the smoothed and unsmoothed monthly data. For graphs including all months (March–October), the reduction is  $1.25^{\circ}$ – $2.75^{\circ}\text{C}$ .

Caveats associated with the convective severe storm report database are discussed in Brooks et al. (2003), Doswell et al. (2005), and Verbout et al. (2006), among many other formal and informal papers. These three studies documented an increase in the number of all severe reports since the mid-1950s—ranging from a factor of 2 to an order of magnitude. Conversely, the annual number of significant severe reports has experienced minimal change during the same time period. Biases in the storm report database have arisen largely from population density variations, differences and trends in local verification efforts/methods, the burgeoning number of storm enthusiasts, and technological advances that make storm reporting easier. Even though the severe storm report database is fraught with uncertainty, the errors most strongly influence time series analyses, which are not being conducted in the present study. Nevertheless, the aforementioned smoothing of  $T_{700}$  and MUCIN is intended to account, in part, for spatial reporting biases that undoubtedly affect the results herein.

It is especially important to emphasize that our study uses severe storms as a rough “proxy” for the occurrence of DMC. Thus, using  $T_{700}$  within the context of this study is conditional upon convective initiation *plus* the accurate reporting of severe weather. This means that if convection developed but did not produce severe weather, then that event would not be included in our database. Furthermore, our database results do not address the precise initiation of convection in time and space, because we did not assess lightning, radar, or satellite data to see where storms first developed. Thus, the report locations may not necessarily indicate where convection developed, but rather where it became severe (e.g., the advection scenario stated at the beginning of section 1). The choice of using severe storm reports instead of DMC-initiation cases is justified by the facts that (i) using  $\sim 300\,000$  severe storm reports

represents a robust statistical sample and (ii) gathering DMC-initiation cases over a 14-yr period would be prohibitive.

Given the above constraints of our study, no attempt was made to stratify  $T_{700}$  by storm type (e.g., supercell versus nonsupercell, tornadic versus nontornadic, etc.), as has been done by other investigators (e.g., Rasmussen and Blanchard 1998). This is beyond the scope of this note, although it may provide useful information, such as possibly illustrating that nonsupercells produce most of the tornadoes when  $T_{700}$  is high (e.g.,  $>15^{\circ}\text{C}$ )—tornadoes that almost exclusively are F0–F1. Last, while  $T_{700}$  distributions were assessed within two different time periods (1800–0600 and 0600–1800 UTC), there was no attempt made to divide storm reports specifically into surface-based and elevated categories. While this too could prove insightful, given that regimes and mechanisms that support DMC and severe weather can be quite different between surface-based and elevated DMC, it was likewise considered to be well beyond the scope of the study.

Finally, another potential concern in the present study is the accuracy and representativeness of the NARR data. Mesinger et al. (2006) reported root-mean-square (RMS) errors of  $0.8^{\circ}$ – $0.9^{\circ}\text{C}$  for  $T_{700}$  when comparing the NARR to radiosondes. We found similar results for Bismarck, North Dakota (BIS), with a bias of  $-0.15^{\circ}\text{C}$  (NARR slightly colder) and a correlation coefficient of 0.993. Additionally, spurious grid-scale precipitation sometimes occurs in the NARR dataset (West et al. 2007), particularly from 2003 onward when the analysis system changed with respect to the input precipitation and ice cover datasets. Reprocessed data from 2003 to 2006 were used herein, but this does not preclude the occurrence of spurious grid-scale precipitation (West et al. 2007). However, only 20% of all reports in this study occurred during 2003–06, and of these only  $\sim 13.5\%$  potentially would be affected by spurious grid-scale precipitation [i.e.,  $<3\%$  of the entire dataset; see West et al. (2007)]. Ultimately, the spatially and temporally consistent NARR dataset was preferred over the relatively coarse network of radiosondes [which have their inherent limitations, e.g., Schwartz and Doswell (1991)] in order to increase the sample size.

### 3. Results and discussion

#### a. $T_{700}$ and all severe storm reports

The results for all severe storm reports show a clear propensity for greater  $T_{700}$  as one goes from lower to higher surface elevations (cf. Figs. 4 and 6), with geographic distributions of  $T_{700}$  mirroring the topography to

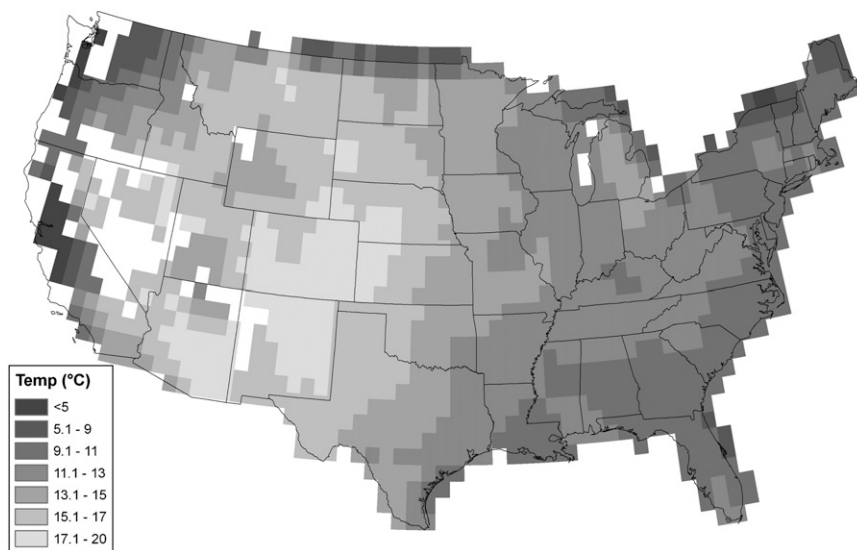


FIG. 6. Maximum  $T_{700}$  ( $^{\circ}\text{C}$ ) associated with all convective severe storm reports from March to October 1993–2006. The maximum  $T_{700}$  was determined from all reports in each of the roughly 80-km grid boxes, and then smoothing was applied by averaging  $3 \times 3$  matrices and assigning the result to the center grid box (see section 2). White boxes denote areas with insufficient data. A color version of this figure is available online (<http://www.crh.noaa.gov/unr/?n=700mbTempsSvr>).

some extent. Indeed, the correlation coefficient between surface elevation (Fig. 4) and the smoothed maximum  $T_{700}$  for all severe storm reports (Fig. 6) is 0.57, which is significantly ( $\alpha < 0.001$ ) different from zero based on a Student's  $t$  test (Wilks 1995). This is not surprising because 700 mb becomes increasingly close to the surface when moving toward higher elevations. Accordingly, the 700-mb level becomes part of the mixed layer at relatively high and arid elevations where sensible heat fluxes can strongly influence  $T_{700}$  (Carlson 1998, 449–457). In such environments, although  $T_{700}$  may often be very high, the capping inversion may not even exist—and if it does, it typically exists above 700 mb.

With regard to nonmountainous areas, the location with the highest  $T_{700}$  exists over the central high plains, from just east of the Front Range to  $100^{\circ}\text{W}$  in Nebraska and Kansas—an area frequently overspread by strong elevated mixed layers (EMLs). Operational experience indicates that very deep/warm boundary layer mixing (to at or above the 700-mb level) is rather common over the high plains with diurnal heating. When coupled with relatively elevated terrain, this is a supportive factor for reducing inhibition and allowing for DMC—despite high  $T_{700}$ . Correlation coefficients between  $T_{700}$  and CIN/LSI (Table 1) at the stations of Denver, Colorado (DNR); Midland, Texas (MAF); and Dodge City, Kansas (DDC), support this notion, with relatively strong correlations at 1200 UTC, but markedly weaker correlations at 0000 UTC (near peak heating). Meanwhile, generally

downstream of this area, the strongest horizontal gradient in maximum  $T_{700}$  exists over the lower and middle Missouri River valley regions. This appears to reflect the relative rarity of deeply mixed boundary layers and the more prohibitive effect of the EML over increasingly lower terrain—necessitating increasingly cooler  $T_{700}$  if DMC is to occur. Correlation coefficients for BIS (just east of the high plains) lend credence to this, with strong correlations between  $T_{700}$  and CIN/LSI (Table 1) that are far less variable throughout the diurnal cycle.

Because the high plains receives a significant fraction of the total severe storm reports in the CONUS (e.g., Brooks et al. 2003; Doswell et al. 2005), this area deserves further investigation. Looking at a subset of the high plains (i.e., the rectangular area in Fig. 4), the frequency of severe reports with  $T_{700} > 12^{\circ}\text{C}$  is a nontrivial 25.7% (Fig. 7). When the June–August period is considered collectively, this frequency rises to 37.4%. Although many of these storms likely are high based, that does not necessarily mean they are elevated whereby their inflow is above a surface-based stable layer (Corfidi et al. 2008). Clearly, if forecasters rely solely on the  $T_{700} > 10^{\circ}\text{--}12^{\circ}\text{C}$  rule of thumb for capping across the high plains, they will be led astray on many occasions.

Further opposing the general rule that  $10^{\circ}\text{--}12^{\circ}\text{C}$  at 700 mb is a limiting factor for DMC, 64% of the area with data in Fig. 6 has maximum  $T_{700} > 12^{\circ}\text{C}$ , covering much of the western and central CONUS. The only place where the larger  $12^{\circ}\text{C}$  guideline consistently applies as an upper

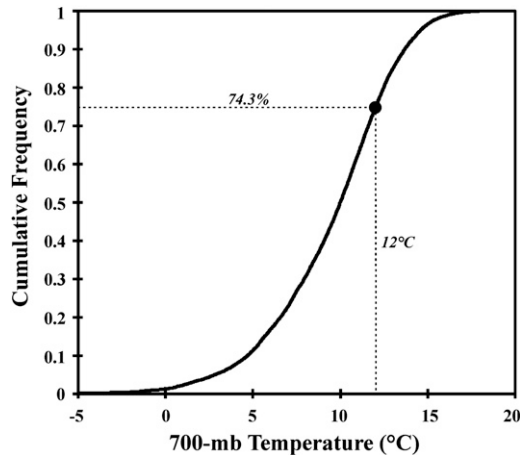


FIG. 7. Empirical cumulative distribution function for  $T_{700}$  associated with all convective severe storm reports in the high plains region outlined in Fig. 4 (28 282 reports, 9.5% of all CONUS reports). The boldface dot signifies that 25.7% of the severe reports are associated with  $T_{700} > 12^{\circ}\text{C}$ .

bound for DMC and severe storms is over (i) the far western CONUS and (ii) the eastern one-quarter of the CONUS. Moreover, 10% of the CONUS—from the high plains to the southern Rockies—has maximum  $T_{700} > 17^{\circ}\text{C}$  (Fig. 6; 15% for the unsmoothed data). Maximum values of  $T_{700}$  from the raw data are  $20.4^{\circ}\text{C}$  for tornadoes,  $20.6^{\circ}\text{C}$  for hail, and  $21.1^{\circ}\text{C}$  for wind. Even the smoothed *average*  $T_{700}$  for the entire dataset has 14% (2%) of the CONUS with temperatures  $>10^{\circ}\text{C}$  ( $>12^{\circ}\text{C}$ ), primarily over the central and southern Rockies (refer to the Fig. 6 caption for an online version of this image)—again illustrating the decreased utility of  $T_{700}$  guidelines within elevated terrain.

Although severe thunderstorm events can occur across a substantial portion of the CONUS with  $T_{700} > 10^{\circ}\text{--}12^{\circ}\text{C}$ , one might argue that this does not happen very often. This is especially true during the cooler months when the 95th percentile of  $T_{700}$  with severe storms is  $5.4^{\circ}\text{C}$  in March,  $7.2^{\circ}\text{C}$  in April, and  $9.0^{\circ}\text{C}$  in October; the maximum  $T_{700}$  for any severe report in March is  $12.2^{\circ}\text{C}$ , and in October it is  $12.4^{\circ}\text{C}$ . However, during the warmest months of July and August the 95th percentiles reach  $13.9^{\circ}$  and  $13.0^{\circ}\text{C}$ , respectively (Fig. 8). What is more,  $T_{700}$  is  $>12^{\circ}\text{C}$  ( $>14^{\circ}\text{C}$ ) for 6.1% (1.8%) of all reports in the CONUS for the dataset herein; in July this increases to 14.1% (4.8%). As indicated by these results, it is essential that seasonal variations in  $T_{700}$  be taken into account when gauging the strength of the capping inversion, which is consistent with Miller's (1967) findings with respect to the  $T_{700}$  rule (recall the discussion in section 1).

The monthly results clearly show the seasonal cycle of maximum  $T_{700}$  associated with severe storm reports,

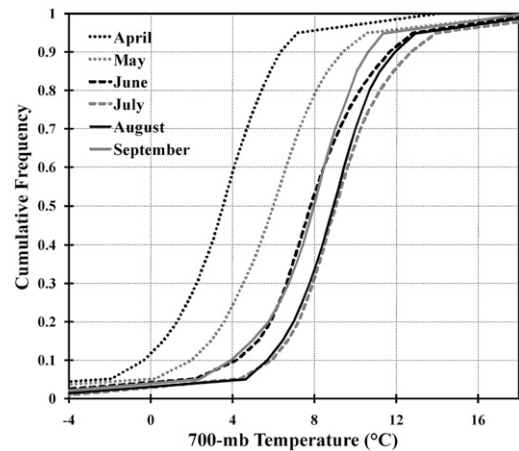


FIG. 8. Empirical cumulative distribution functions for  $T_{700}$  associated with all convective severe storm reports across the CONUS from 1993 to 2006 for each of the months from April to September.

which is most conspicuous across the central CONUS (Fig. 9). As expected, this mirrors the climatology of environmental  $T_{700}$ , with the highest values occurring during the warmest time of the year. This annual oscillation of maximum  $T_{700}$ —along with that shown in Fig. 8—is in accord with the general seasonal guidelines for  $T_{700}$  and capping proposed by Davies (2009); although, geographic variations at a given time must concurrently be considered. As in Fig. 6, the highest values of  $T_{700}$  from month to month consistently are located over the central Rockies and high plains; during July an area of smoothed maximum  $T_{700} > 15^{\circ}\text{C}$  extends from Canada to Mexico (Fig. 9d). The spread of smoothed maximum  $T_{700}$  among various months also is largest over the high plains (e.g.,  $\sim 11.5^{\circ}\text{C}$  difference between April and July over eastern Colorado) compared to areas such as the southeastern CONUS (e.g.,  $\sim 3^{\circ}\text{C}$  difference between April and July over Georgia). Again, this is a reflection of the EML that climatologically originates over the central and southern Rocky Mountains and passes over the high plains, yet infrequently reaches the eastern CONUS (Carlson 1998, 462–463).

The diurnal cycle of  $T_{700}$  is dominated by severe storm reports from 1800 to 0600 UTC; 84.2% fall within this time frame, which has a smoothed maximum  $T_{700}$  pattern nearly identical to Fig. 6. However, a notable diurnal difference still emerges whereby the maximum  $T_{700}$  is lower during 0600–1800 UTC than during 1800–0600 UTC (refer to the Internet address in the Fig. 6 caption for these images). The difference is by far most apparent across the high plains, where differences in maximum  $T_{700}$  between these two time periods range from  $2^{\circ}$  to  $8^{\circ}\text{C}$ . This may reflect the strong capping

### Smoothed Maximum 700-mb Temperature (All Severe Reports, Apr–Sep, 1993–2006)

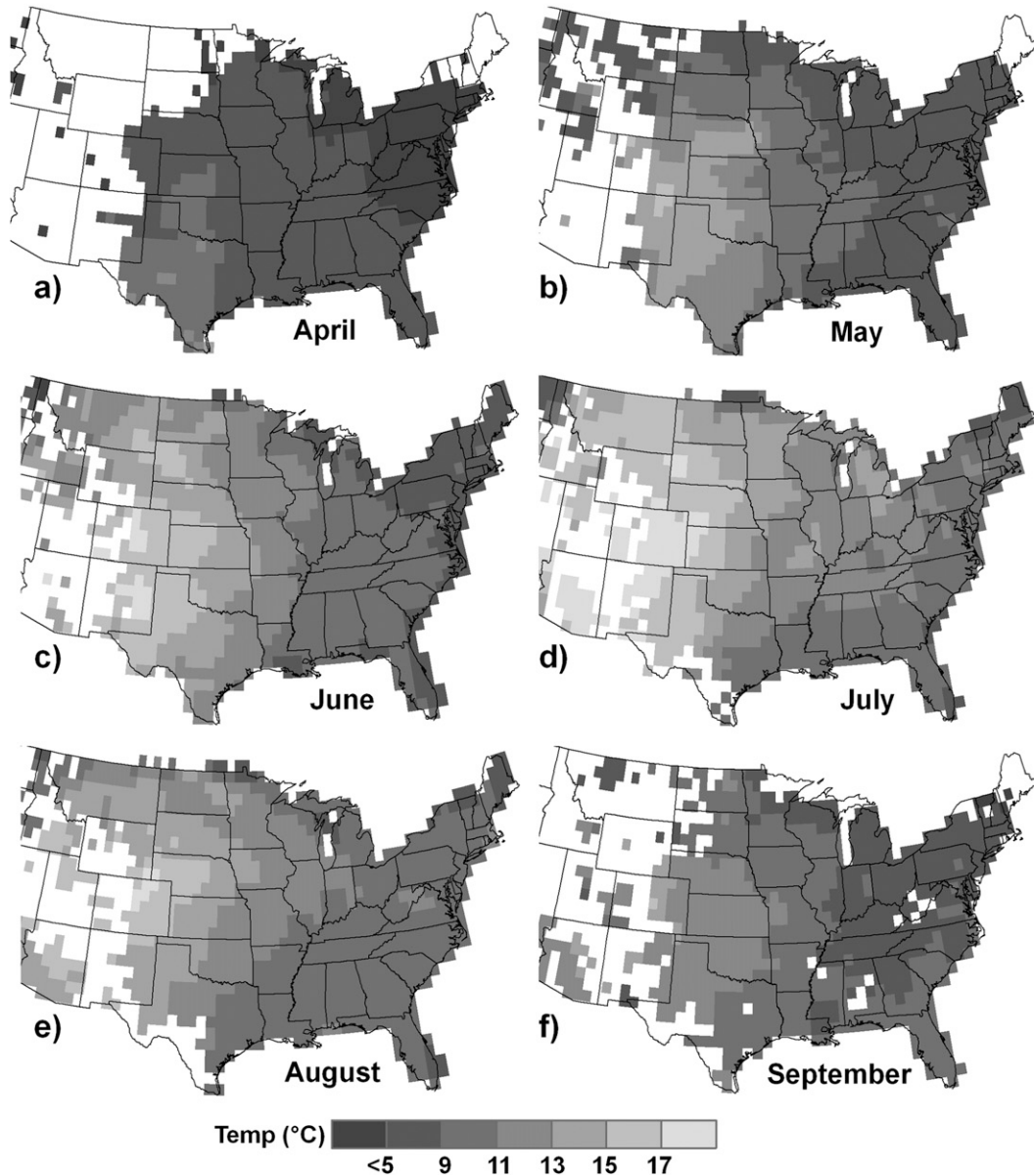


FIG. 9. As in Fig. 6, but for monthly climatologies including (a) April, (b) May, (c) June, (d) July, (e) August, and (f) September.

EMLs that can be overcome during the day by deeply mixed boundary layers on elevated terrain; comparatively, with near-surface stabilization common after dark, markedly “cooler” capping aloft (e.g.,  $T_{700}$ ) is required in order to initiate or maintain DMC over the same areas. Meanwhile, across the eastern half of the CONUS the differences generally are  $1^{\circ}$ – $2^{\circ}\text{C}$  (i.e., higher during 1800–0600 UTC). And for average  $T_{700}$  the diurnal differences

are  $\pm 1^{\circ}$ – $2^{\circ}\text{C}$  for nearly all of the central and eastern CONUS. Comparisons cannot be made across most of the Rocky Mountains because of the dearth of reports there between 0600 and 1800 UTC.

In summary, results presented in this section elucidate that (i) the relationship between  $T_{700}$  and the occurrence of severe convective storms is strongly tied to topography and (ii) values of  $T_{700} > 10^{\circ}$ – $12^{\circ}\text{C}$  are not

### Smoothed Maximum 700-mb Temperature (Torn, Hail, & Wind, Apr–Sep, 1993–2006)

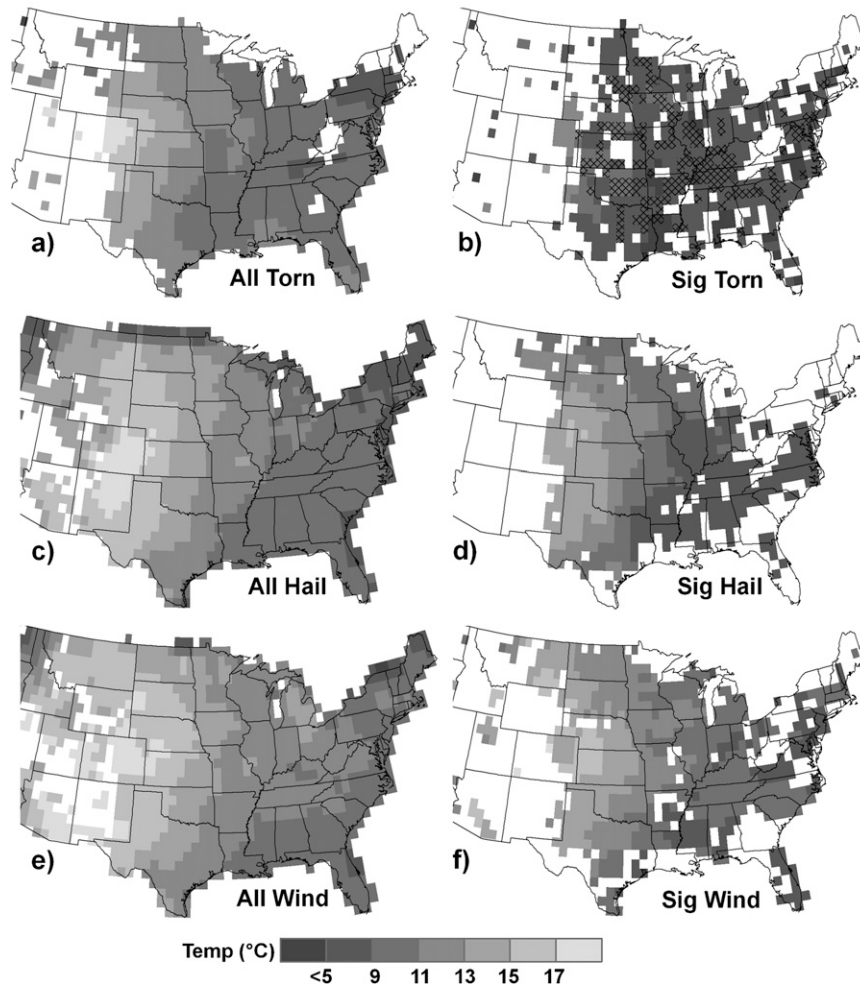


FIG. 10. As in Fig. 6, but for partitions based on report type including (a) all tornadoes, (b) significant tornadoes, (c) all hail, (d) significant hail, (e) all wind, and (f) significant wind. Recall that only one report was required per grid box for the significant tornadoes [(b)], and thus these results should be interpreted with caution; if five reports per grid box would have been used, then the area of (b) would only be 27% of its current size (see cross-hatched area; refer to section 2 for additional discussion).

uncommon in severe thunderstorm environments, especially across the high plains and Rocky Mountains from late May through August.

#### *b. $T_{700}$ versus severe storm report type*

Variations in maximum  $T_{700}$  are discernible among the three different severe storm report types, as well as between the significant and nonsignificant categories (e.g., Fig. 10). First, it is evident that the smoothed maximum  $T_{700}$  generally increases from tornadoes to hail, and from hail to wind. The differences are mainly from 1° to 3°C across the central CONUS for tornadoes

and hail (cf. Figs. 10a and 10c), but are smaller for hail and wind with 0°–2°C increases in the smoothed maximum  $T_{700}$  for wind over the central and eastern CONUS (cf. Figs. 10c and 10e). The exception is Florida, where this trend is reversed with a 1°–2°C decrease from tornadoes to wind. Second, similar changes/increases in the smoothed maximum  $T_{700}$  are observed among the significant tornado, hail, and wind categories (Figs. 10b, 10d, and 10f). However, in this case the increase of maximum  $T_{700}$  is larger from significant tornadoes to significant hail (i.e., 1°–6°C) than it is for all tornadoes to all hail, with the largest increases (3°–6°C) confined primarily to the central CONUS.

The distribution of the raw severe storm reports versus  $T_{700}$ —grouped into classes according to damage/severity (Fig. 11)—supports the trends noted above. Specifically, the maximum  $T_{700}$  values increase for each category from tornado to hail to wind. Furthermore, the decile plots show a contraction of the distributions from the less damaging/weaker events (left side of Fig. 11) to the most damaging/strongest events (right side of Fig. 11). Not only does the maximum  $T_{700}$  decrease with increasing damage/severity of the reports (as was the case in Fig. 10), but the minimum  $T_{700}$  increases concurrently, primarily for tornado and hail reports. Junker et al. (1999) similarly found that none of their extreme convective heavy rainfall events occurred with  $T_{700} > 12^{\circ}\text{C}$ , even though some lesser intensity events did occur with  $T_{700}$  from  $12^{\circ}$  to  $15^{\circ}\text{C}$ .

Another interesting aspect of Fig. 11 is the clustering of the middle 80% of the distributions: (i)  $1.5^{\circ}$ – $11^{\circ}\text{C}$  for tornadoes, (ii)  $1^{\circ}$ – $12^{\circ}\text{C}$  for hail, and (iii)  $3^{\circ}$ – $13^{\circ}\text{C}$  for wind. From this perspective it becomes apparent why the  $10^{\circ}$ – $12^{\circ}\text{C}$  threshold for DMC gained support (the caveats associated with using severe storm reports as a proxy for DMC notwithstanding); 90% of the distributions are below  $12^{\circ}$ – $13^{\circ}\text{C}$ , concordant with Johns and Doswell's (1992) statement in section 1. Furthermore, no F4–F5 (F2–F3) tornadoes were recorded with  $T_{700} > 12^{\circ}\text{C}$  ( $>14^{\circ}\text{C}$ ), and only 5% of all tornadoes from 1993 to 2006 are associated with  $T_{700} > 12^{\circ}\text{C}$  (6.8% and 5.6% for all hail and wind, respectively). This amounts to an average of just 54 out of 1092 tornadoes per year with  $T_{700} > 12^{\circ}\text{C}$ . By way of comparison, the frequencies of  $T_{700} > 12^{\circ}\text{C}$  with significant tornadoes, significant hail, and significant wind are 2.6%, 9.0%, and 11.3%, respectively. Conditional upon a reported tornado, the empirical probability of a significant tornado is  $\sim 0.1\%$  when  $T_{700} > 12^{\circ}\text{C}$ . Keep in mind, however, that Fig. 11 is based on the entire dataset; again,  $T_{700}$  distributions vary substantially based on factors like surface elevation and time of year (e.g., refer to Figs. 6–8).

There is at least some physical explanation for the above observations. First, with respect to wind production, steep low-level lapse rates favor the downward transport of vertical momentum (e.g., Wakimoto 1985). Therefore,  $T_{700}$  can be rather high, but if the capping inversion has been eroded (via boundary layer heating) and DMC is produced (e.g., Fig. 5a), severe wind-producing storms, such as dry microbursts, can result. Even derechos (i.e., widespread, damaging convective windstorms) can occur when the average  $T_{700}$  is relatively high (e.g., Johns and Hirt 1987), with the climatological maximum of derechos along the northeastern edge of the warmest  $T_{700}$ . Second, the development of severe hail requires large buoyancy for strong updrafts, as well as a melting level

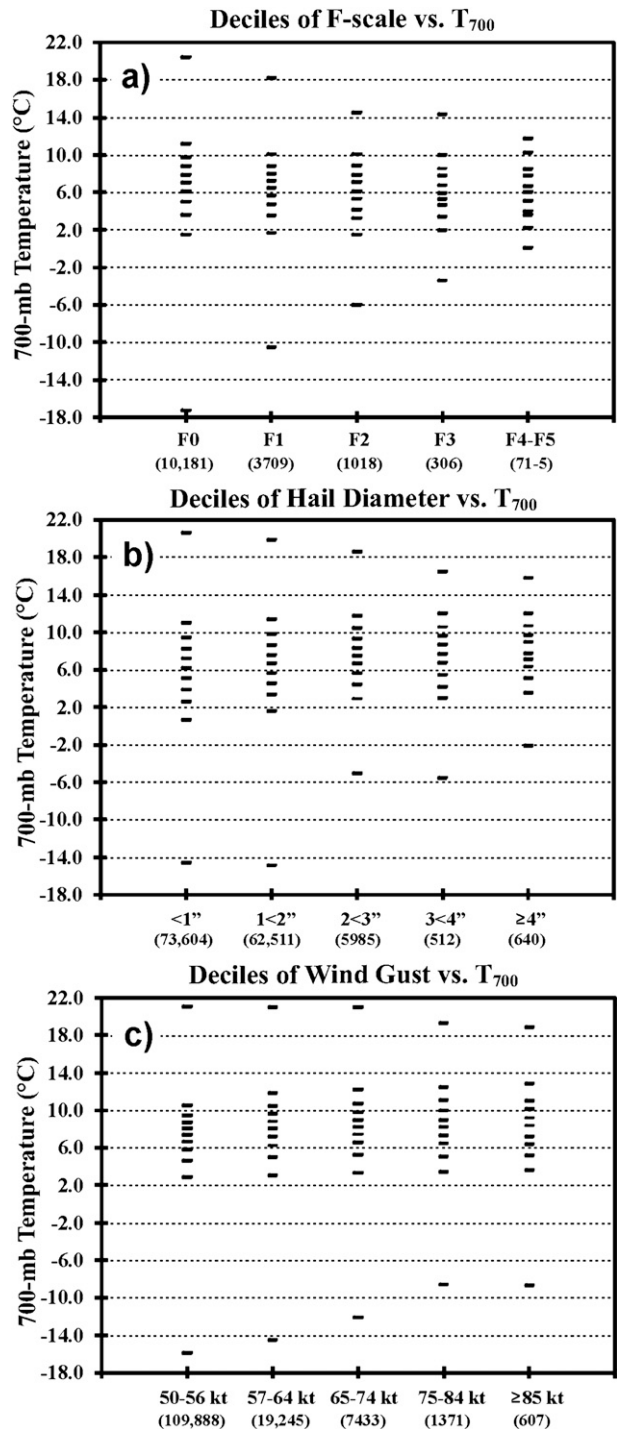


FIG. 11. Decile plots (i.e., dashes every 0%, 10%, . . . , 100%) for report-type partitions vs  $T_{700}$  for (a) tornado rating, (b) hail diameter (1 in. = 2.54 cm), and (c) wind gust (1 kt =  $0.5144 \text{ m s}^{-1}$ ). Values in parentheses indicate the total number of CONUS-wide reports for that specific partition (e.g., there are 1018 tornadoes rated F2 from 1993 to 2006).

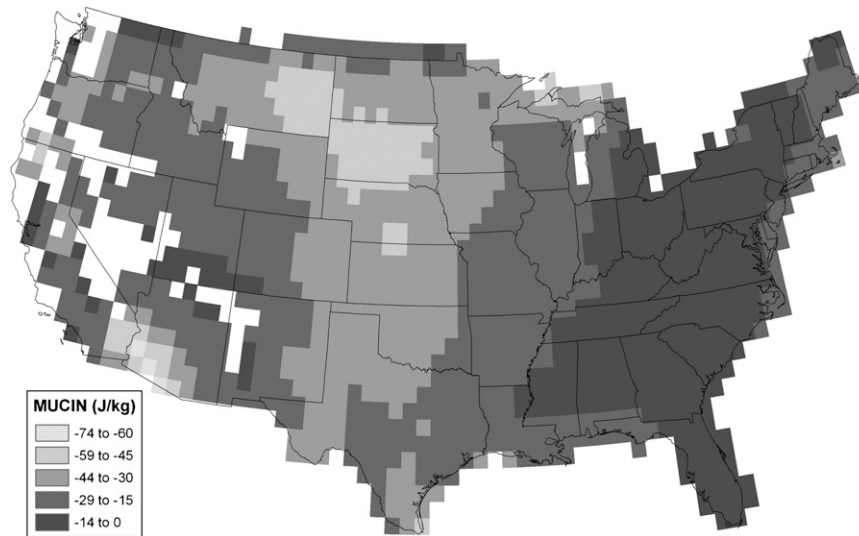


FIG. 12. As in Fig. 6, but for average NARR MUCIN associated with all convective severe storm reports from March to October, 1993–2006.

that is not exceedingly high above the ground (e.g., Knight and Knight 2001). As buoyancy diminishes and the melting level increases above a given threshold (which is typical of environments with high  $T_{700}$ ), the proclivity for severe hail wanes. This suggests that  $T_{700}$  would not be as high, on average, for severe-hail environments compared to severe-wind environments (or for significant severe hail versus all severe hail). Last, recent research suggests that both low lifted condensation level (LCL) and low LFC heights are more favorable for tornadogenesis than high LCL and LFC heights, especially for significant tornadoes (e.g., Rasmussen and Blanchard 1998; Thompson et al. 2003; Davies 2004). To attain low LCL heights, and also reduce CIN and lower LFC heights such that the environment is strongly surface based, in the presence of high  $T_{700}$ , a rather large value of low-level  $\theta_e$  is needed. This is not a routine occurrence in the atmosphere; hence, tornadic storms, relative to severe hail- and wind-producing storms, tend to favor environments with lower  $T_{700}$  where collocated low-LCL and low-CIN environments are more attainable.<sup>4</sup>

In summary, as  $T_{700}$  increases, DMC and severe storms are less likely to be sustained and/or remain strongly surface based in environments with low LCL heights (which tend to favor tornadogenesis). And as  $T_{700}$

increases further, production of severe hail is less efficient because of melting and possibly less buoyancy. Moreover, the maximum  $T_{700}$  is lower for significant severe reports versus all severe reports, and especially for significant tornadoes versus all tornadoes.

### c. MUCIN and severe storm reports

Only a small subset of the MUCIN results is presented here because these results are not the focus of the present study. However, considerable additional information is available at the Internet address provided in the Fig. 6 caption. The intent here is only to point out the most apparent contrasts between using  $T_{700}$  and CIN when determining characteristics of the capping inversion.

Consistent among all of the MUCIN versus severe storm report results is a maximum of absolute values across the central CONUS, whether this is for minimum MUCIN<sup>5</sup> or for average MUCIN (e.g., Fig. 12). It is likely that this climatological extreme in MUCIN (and capping) is a result of the advection of the EML over the central CONUS—producing the familiar “loaded gun” type I sounding (Miller 1967). These results are consistent with Graziano and Carlson (1987), and are not

<sup>4</sup> Although it is beyond the scope of this study, it is possible that the difference between Figs. 10a and 10b represents two different tornadogenesis processes in the high plains: nonsupercell tornadoes in the warmer  $T_{700}$  environments (Fig. 10a) versus supercell tornadoes in the cooler  $T_{700}$  environments (Fig. 10b). Nonsupercell tornadoes can occur with relatively high cloud bases and LCL heights—a condition presumably more common when  $T_{700}$  is high.

<sup>5</sup> The online minimum MUCIN graphics display absolute values that are very large in some locations ( $< -300$  to  $-400$   $\text{J kg}^{-1}$ ), particularly in the plains states. Although severe storms do occur on occasion in these hostile environments, it is important to note that the most unstable parcel (i.e., the parcel with the highest  $\theta_e$ ) does not always correspond to the parcel with the least amount of CIN (e.g., Fig. 14). Therefore, some of the extreme MUCIN values may not necessarily correspond to the parcels that resulted in DMC.

surprising given the geography of the western and central CONUS (Carlson 1998).

Like for  $T_{700}$ , there is a significant, albeit somewhat weaker, correlation between elevation and the smoothed minimum MUCIN ( $r = 0.44$ ; also cf. Figs. 4 and 12), meaning that as elevation increases, the strength of the capping generally decreases. After closer inspection it appears this correlation coefficient is misleading, however, as average MUCIN becomes stronger/more negative from the eastern CONUS to the central CONUS (Fig. 12)—suggesting the correlation is negative in this area. In fact, the correlation coefficient between elevation and minimum MUCIN is  $-0.25$  when conditional on elevation  $<750$  m; this region comprises mainly the eastern half of the CONUS and a narrow zone along the West Coast (refer to Fig. 4). On the other hand, the correlation coefficient is  $0.55$  when conditional on elevation  $>750$  m. In agreement with these results, the scatterplot of these two variables is conspicuously non-linear (not shown). This pattern differs from what was shown for smoothed maximum  $T_{700}$  (Fig. 6), where the largest values were shifted unequivocally toward the highest terrain. This dichotomy reinforces that, despite its location well downstream of the highest  $T_{700}$  often present over the Rockies, the central CONUS experiences the highest frequency of substantial-CIN environments due to the nature of the EML.

Another contrast between the results of  $T_{700}$  and MUCIN is that the seasonality of MUCIN is much less pronounced (e.g., Fig. 13); the patterns of MUCIN show minimal contrast among the monthly curves from April to September. Likewise, Graziano and Carlson (1987) found little seasonal variation for critical values of the LSI, except for slightly higher values during the early spring. This result should be expected for a physically based measure of the capping inversion such as CIN and LSI. Note also that the cumulative distribution functions (CDFs) are of exponential type in Fig. 13, indicating that most of the severe events occurred with relatively small capping. Indeed, 70% of the CONUS events occurred with MUCIN between  $-24.0$  and  $0 \text{ J kg}^{-1}$ , which is consistent with the discussion of boundaries and CIN in section 1. Compare this to Fig. 8 where the CDFs rise sharply after they reach a given threshold and then tail off gradually for extreme values of  $T_{700}$ .

The last distinction to be drawn between  $T_{700}$  and MUCIN is the diurnal variation. Although values of  $T_{700}$  are smaller during 0600–1800 UTC (suggesting weaker capping aloft), MUCIN actually becomes stronger overnight, especially across the central CONUS. Similarly, Graziano and Carlson (1987) noted LSIs were slightly higher at 1200 UTC relative to other times. We believe this is a consequence of nocturnal cooling in the boundary

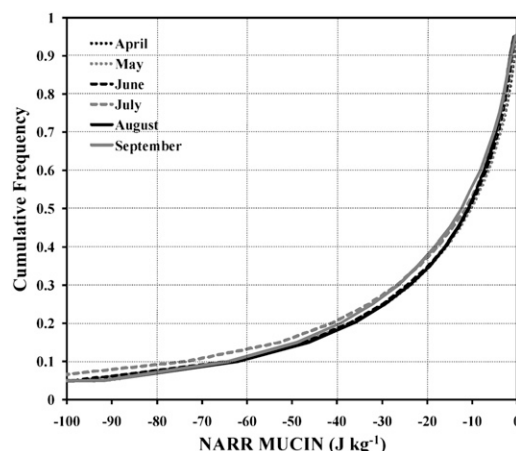


FIG. 13. As in Fig. 8, but for NARR MUCIN.

layer beneath air with relatively high values of  $T_{700}$  associated with the EML, which results in climatologically stronger CIN at night. The fact that severe storms—perhaps mostly elevated—can still occur in the presence of this significant CIN overnight may be related to strengthening of the nocturnal low-level jet and its ability to act as a strong lifting mechanism (e.g., Bonner 1966).

In summary, with respect to convective severe storm reports, it is evident that CIN is (i) climatologically strongest in the central CONUS—consistent with prior research, (ii) generally a more reliable indicator of the capping inversion than  $T_{700}$ , and (iii) not as strongly dependent upon elevation or time of year as  $T_{700}$ , but does vary more diurnally (especially over the plains).

#### 4. Conclusions and summary

The main emphasis of the present study was to compare  $T_{700}$  with convective severe storm reports across the CONUS. Admittedly, this is a straightforward study, but one that needs to be done nonetheless considering the continued application of  $T_{700}$  to capping and DMC. Based on the above results, the following conclusions are drawn:

- $T_{700}$  should not be used as a primary guide for forecasting the initiation of DMC or the occurrence of severe storm events, but may have worthwhile utility—when used within the framework of larger conceptual models and “rough” seasonal guidelines—to aid in forecasting the strength of the capping inversion.
- Many areas of the CONUS, especially the Rockies and high plains from late May through August, experience DMC and severe convective storms with  $T_{700}$  above the  $10^{\circ}$ – $12^{\circ}$ C rule of thumb.

- CIN is a much more reliable indicator of the capping inversion than is  $T_{700}$ , although the lack of denser upper-air observations and the inherent deficiencies of numerical models can serve as limitations when attempting to anticipate CIN.

There are several reasons why  $T_{700}$  can fail at defining the capping inversion. First, the thermodynamic profile below the capping inversion in the boundary layer is critical to assessing whether DMC can develop. In particular, changes in moisture quality and mixing depth within the boundary layer can result in varying thresholds for  $T_{700}$  (assuming the LCL is below 700 mb). For example, if the boundary layer is relatively dry and/or shallow, with low  $\theta_e$ , it may be difficult for a parcel to possess small CIN—no matter how low the  $T_{700}$  might be (e.g., Fig. 5b). However,  $T_{700}$  can be very high, but if the atmosphere is deeply mixed and the boundary layer  $\theta_e$  is sufficient to produce positive buoyancy (e.g., Fig. 5a), DMC can develop. Second, on the elevated terrain of the Rocky Mountains and high plains, 700 mb is closer to the ground—if not actually part of the mixed layer. Thus, despite environments commonly characterized by high  $T_{700}$ , CIN can be minimized and DMC may occur. Third, DMC may initiate above the 700-mb level in the form of elevated thunderstorms (e.g., Fig. 14, 661 mb). In this instance it makes no sense to view  $T_{700}$  to determine the amount of capping.

Additionally, the strength of the mesoscale and smaller-scale forcing determines how high a parcel can be lifted. With weak (strong) forcing, it will be relatively difficult (easy) for a parcel to reach the LFC even if the  $T_{700}$  is low (high). There are certainly many instances in which weak-CIN environments do not produce DMC, while, in contrast, strong mesoscale forcing mechanisms can sometimes overcome strong capping and allow the initiation of DMC. In the same vein, ongoing convective systems with intense cold pools (e.g., the previously discussed derechos) can likewise overcome significant CIN through vigorous lifting along gust fronts (recall the very large negative MUCIN values mentioned in footnote 5). Clearly, manifold components—not necessarily independent of one another—need to be considered when assessing the capping inversion.

Considerable evidence has been presented herein to discourage the exclusive use of  $T_{700}$  to assess the extent and strength of the capping inversion. Nevertheless, there may be times when this simple variable might be beneficial as an adjunct when assessing the capping inversion, as well as a tool for monitoring the spatial extent of the EML. For example, at long forecast projections (e.g., >24–36 h) when the boundary layer profile is not well forecast, it may behoove a forecaster to look at  $T_{700}$

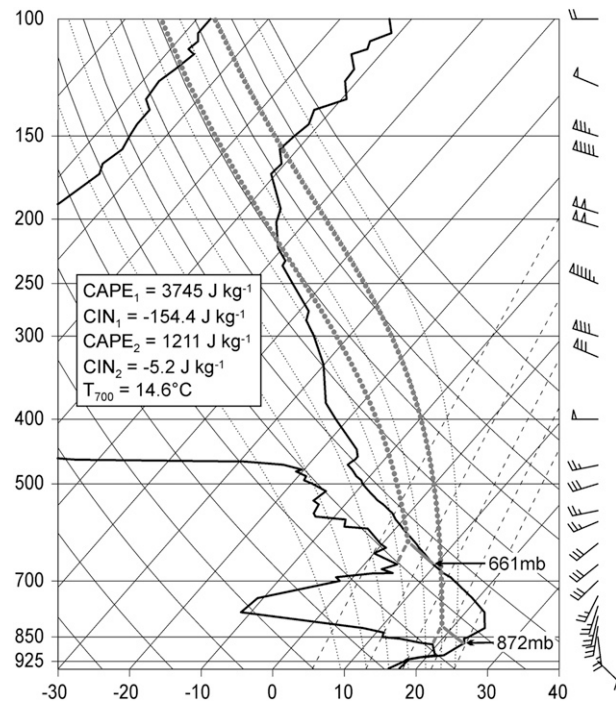


FIG. 14. Observed skew  $T$ - $\log p$  sounding (thick black lines) for Bismarck, ND, valid 1200 UTC 13 Aug 2007, similar to Fig. 2. The ascent for the most unstable parcel lifted from the 872-mb level ( $\text{CAPE}_1$  and  $\text{CIN}_1$ ) is highlighted by the thick gray lines. Similarly, the ascent is highlighted for a parcel lifted from the 661-mb level ( $\text{CAPE}_2$  and  $\text{CIN}_2$ ). (DMC initiated within 55 km of this sounding at 1300 UTC; severe DMC occurred both 150 km north of BIS and 100 km southeast of BIS from 1245 to 1600 UTC.)

to get an estimate of the capping inversion based on the time of year and location in the CONUS, capitalizing on the climatology that has been presented here. Another situation when  $T_{700}$  potentially may be useful is by comparing values of  $T_{700}$  to severe storm reports from the previous day, and then using that as a general guideline for the current day's forecast for the same geographic area—assuming the boundary layer has not changed appreciably. In summary, forecasting capping, DMC, and severe storms may be assisted by consulting  $T_{700}$  from the perspective of climatology and tracking the EML, but the physically relevant variables (e.g., CIN) and methods (e.g., sounding analysis) should take precedence over  $T_{700}$ .

*Acknowledgments.* We are indebted to the following individuals for their help with this research project: (i) Steve Byrd, Stephen Corfidi, Dan Lindsey, Bob Maddox, and Steve Weiss for providing background information and references; (ii) Phil Schumacher for his support with GEMPAK and NARR data, as well as for his early discussions on this project; (iii) Al Pietrycha for

providing the data for Fig. 1; (iv) Geoff Manikin for providing information on the NARR MUCIN calculations; (v) Jon Davies, Chuck Doswell, Roger Edwards, Jonathan Garner, Patrick Kerrin, Jeff Passner, Harald Richter, Glen Romine, Jeff Snyder, Greg Stumpf, and Rich Thompson for correspondence on the usage of 700-mb temperatures for capping; and (vi) Kyle Carstens, Eric Helgeson, Jeff Johnson, Jeff Manion, Paul Smith, Jon Zeitler, and two anonymous reviewers for providing a review of this manuscript. We also would like to thank Dave Carpenter (meteorologist in charge, WFO Rapid City, South Dakota) for supporting this work.

## REFERENCES

- Ashley, W. S., A. J. Krmenc, and R. Schwantes, 2008: Vulnerability due to nocturnal tornadoes. *Wea. Forecasting*, **23**, 795–807.
- Bikos, D., J. Weaver, and B. Motta, 2002: A satellite perspective of the 3 May 1999 Great Plains tornado outbreak within Oklahoma. *Wea. Forecasting*, **17**, 635–646.
- Bonner, W. D., 1966: Case study of thunderstorm activity in relation to the low-level jet. *Mon. Wea. Rev.*, **94**, 167–178.
- Brooks, H. E., C. A. Doswell III, and M. P. Kay, 2003: Climatological estimates of local daily tornado probability for the United States. *Wea. Forecasting*, **18**, 626–640.
- Byrd, S. F., 1993: An examination of downbursts in the eastern Great Plains associated with a very warm mid-level environment. NOAA Tech. Memo. CR-102, St. Louis, MO, 208–219. [Available from NWS Central Region Headquarters, 7220 NW 101st Terrace, Kansas City, MO 64153.]
- Carlson, T. N., 1998: *Mid-Latitude Weather Systems*. Amer. Meteor. Soc., 507 pp.
- , R. A. Anthes, M. Schwartz, S. G. Benjamin, and D. G. Baldwin, 1980: Analysis and prediction of severe storms environment. *Bull. Amer. Meteor. Soc.*, **61**, 1018–1032.
- Colby, F. P., Jr., 1984: Convective inhibition as a predictor of convection during AVE-SESAME II. *Mon. Wea. Rev.*, **112**, 2239–2252.
- Corfidi, S. F., S. J. Corfidi, and D. M. Schultz, 2008: Elevated convection and castellanus: Ambiguities, significance, and questions. *Wea. Forecasting*, **23**, 1280–1303.
- Davies, J. M., 2004: Estimations of CIN and LFC associated with tornadic and nontornadic supercells. *Wea. Forecasting*, **19**, 714–726.
- , cited 2009: 700mb temperatures as a rough estimation of the “cap” regarding initiation of severe convection. [Available online at <http://www.jondavies.net/700mbTcap/700mbTcap.htm>.]
- Doswell, C. A., III, and E. N. Rasmussen, 1994: The effect of neglecting the virtual temperature correction on CAPE calculations. *Wea. Forecasting*, **9**, 625–629.
- , H. E. Brooks, and M. P. Kay, 2005: Climatological estimates of daily local nontornadic severe thunderstorm probability for the United States. *Wea. Forecasting*, **20**, 577–595.
- Graziano, R. H., and T. N. Carlson, 1987: A statistical evaluation of lid strength on deep convection. *Wea. Forecasting*, **2**, 127–139.
- Hales, J. E., Jr., 1988: Improving the watch/warning program through use of significant event data. Preprints, *15th Conf. on Severe Local Storms*, Baltimore, MD, Amer. Meteor. Soc., 165–168.
- Hart, J. A., 1993: SVRPLLOT: A new method of accessing and manipulating the NSSFC severe weather database. Preprints, *17th Conf. Severe Local Storms*, St. Louis, MO, Amer. Meteor. Soc., 40–41.
- Johns, R. H., and W. D. Hirt, 1987: Derechos: Widespread convectively induced windstorms. *Wea. Forecasting*, **2**, 32–49.
- , and C. A. Doswell III, 1992: Severe local storms forecasting. *Wea. Forecasting*, **7**, 588–612.
- Junker, N. W., R. S. Schneider, and S. L. Fauver, 1999: A study of heavy rainfall events during the Great Midwest flood of 1993. *Wea. Forecasting*, **14**, 701–712.
- Kalthoff, N., and Coauthors, 2009: The impact of convergence zones on the initiation of deep convection: A case study from COPS. *Atmos. Res.*, **93**, 680–694.
- Knight, C. A., and N. C. Knight, 2001: Hailstorms. *Severe Convective Storms. Meteor. Monogr.*, No. 50, Amer. Meteor. Soc., 223–254.
- McNulty, R. P., 1995: Severe and convective weather: A central region forecasting challenge. *Wea. Forecasting*, **10**, 187–202.
- Means, L. L., 1952: On thunderstorm forecasting in the central United States. *Mon. Wea. Rev.*, **80**, 165–189.
- Mesinger, F., and Coauthors, 2006: North American Regional Reanalysis. *Bull. Amer. Meteor. Soc.*, **87**, 343–360.
- Miller, R. C., 1967: Notes on analysis and severe-storm forecasting procedures of the Military Weather Warning Center. Air Weather Service Tech. Rep. 200, Air Weather Service, Scott Air Force Base, IL, 140 pp.
- Moller, A. R., 2001: Severe local storms forecasting. *Severe Convective Storms, Meteor. Monogr.*, No. 50, Amer. Meteor. Soc., 433–480.
- Rasmussen, E. N., and D. O. Blanchard, 1998: A baseline climatology of sounding-derived supercell and tornado forecast parameters. *Wea. Forecasting*, **13**, 1148–1164.
- Schaefer, J. T., 1986: Nocturnal thunderstorms, sometimes known as MCC’s (Mesoscale Convective Complexes). NOAA/NWS CR Tech. Attach. 86-18, 10 pp. [Available from NWS Central Region Headquarters, 7220 NW 101st Terrace, Kansas City, MO 64153.]
- Schwartz, B. E., and C. A. Doswell III, 1991: North American radiosonde observations: Problems, concerns, and a call to action. *Bull. Amer. Meteor. Soc.*, **72**, 1885–1896.
- Thompson, R. L., R. Edwards, J. A. Hart, K. L. Elmore, and P. Markowski, 2003: Close proximity soundings within supercell environments obtained from the Rapid Update Cycle. *Wea. Forecasting*, **18**, 1243–1261.
- Verbout, S. M., H. E. Brooks, L. M. Leslie, and D. M. Schultz, 2006: Evolution of the U.S. tornado database: 1954–2003. *Wea. Forecasting*, **21**, 86–93.
- Wakimoto, R. M., 1985: Forecasting dry microburst activity over the high plains. *Mon. Wea. Rev.*, **113**, 1131–1143.
- , and H. V. Murphey, 2009: Analysis of a dryline during IHOP: Implications for convective initiation. *Mon. Wea. Rev.*, **137**, 912–936.
- Weckwerth, T. M., and D. B. Parsons, 2006: A review of convection initiation and motivation for IHOP\_2002. *Mon. Wea. Rev.*, **134**, 5–22.
- West, G. L., W. J. Steenburgh, and W. Y. Y. Cheng, 2007: Spurious grid-scale precipitation in the North American Regional Reanalysis. *Mon. Wea. Rev.*, **135**, 2168–2184.
- Wilks, D. S., 1995: *Statistical Methods in the Atmospheric Sciences*. Academic Press, 467 pp.